

Horizontal oscillation of a capillary bridge between a spherical grain and a flat surface

Grisel Rojas, Andrea Fabiana Vallone, Rodolfo Omar Uñac, and Ana María Vidales

Instituto de Física Aplicada, CONICET, Universidad Nacional de San Luis, Ejército de los Andes 950, 5700 San Luis, Argentina

Abstract. A granular system's behaviour can be significantly altered by humidity, as even small amounts of condensed liquid between grains affect particle movement. Capillary bridges form between grains, creating cohesive forces that hold particles together, particularly in the pendular state at low saturation. When shearing is applied to granular packing, these bridges deform, with their force depending on their shape, fluid properties, and particle velocity. This makes studying the deformation of liquid bridges crucial for modelling wet granular materials. This study examines the dynamic behaviour of a capillary bridge between a flat surface and a spherical particle using ethylene glycol as the liquid. The deformation is induced by oscillating the horizontal surface while keeping the sphere fixed, causing the meniscus geometry to change. High-speed video captures the deformation, allowing the measurement of advancing and receding contact angles. The angles' behaviour is analysed as a function of the capillary number for a given amplitude and frequency. The research seeks to identify differences in receding and advancing angles, supporting predictions from theoretical models about torsional motion on a liquid film. The limitations of these models are discussed.

1 Introduction

The collective movement of granular materials continues to present significant challenges. Advances in contact laws governing particle-particle and particle-wall interactions have enhanced both the theoretical and numerical descriptions of bulk granular motion. These improvements have led to the development of successful models that are widely used to predict grain behaviour across a variety of scenarios [1]. These models generally assume elastic behaviour for dry solid bodies in contact, where the force-deformation response can be either linear or nonlinear, depending on the materials involved [1-3].

The introduction of moisture further complicates the system, as even small amounts of condensed liquid between grains can dramatically alter the behaviour. Capillary bridges that form between the particles generate cohesive forces, particularly at low saturation levels, where the pendular state dominates. When a granular packing is subjected to shearing or vibration, the continuous deformation of these capillary bridges induces tensile capillary forces and capillary torques. The magnitude of these effects depends on the shape, volume, fluid properties, and the relative velocities of the interacting particles.

In recent decades, models incorporating capillary effects have provided valuable insights into the behaviour of wet granular matter, yielding predictive results with high accuracy [4-8]. Marshall [9] conducted a theoretical analysis of capillary torques acting on a spherical particle rolling on a flat surface coated with a thin liquid film. This study assumed that the capillary number was sufficiently small to approximate the liquid

bridge as having a circular cross-section. He compared the theoretical torque values to experimental measurements by Schade and Marshall [10], as a function of the capillary number. Marshall employed the Cox-Voinov law [11, 12] to approximate the advancing and receding liquid-gas contact angles involved in the analysis.

Building on these prior studies, we aim to extend the understanding of capillary bridge deformation in the presence of torques. Specifically, we focus on the direct observation of a capillary bridge formed between a spherical particle and a flat surface subjected to sinusoidal horizontal oscillation, while the sphere remains fixed. This motion induces a changing meniscus geometry over time. We investigate the behaviour of the bridge geometry as a function of the capillary number, searching for evidence that the receding angle may exhibit distinct behaviour from the advancing angle. This observation aligns with theoretical predictions regarding the torsional motion of grains on a liquid film. Finally, we discuss the limitations of existing models, particularly in relation to the capillary number range explored in our experiments.

2 Experimental setup and methodology

The experiment consists of horizontally vibrating a liquid bridge formed between a fixed sphere and a moving platform. Figure 1 illustrates the experimental setup. A known volume of ethylene glycol ($V = 50 \mu\text{l}$, $\rho = 1.11 \text{ g/cm}^3$) is placed on the surface of an aluminium plate. Then, a spherical plastic particle with a diameter

of 6 mm and adhered to a metallic axis with a plastic support is moved vertically and carefully centred into contact with the liquid. A second smaller particle is glued to the horizontal surface as a reference for determining the movement of the spherical particle relative to the platform.

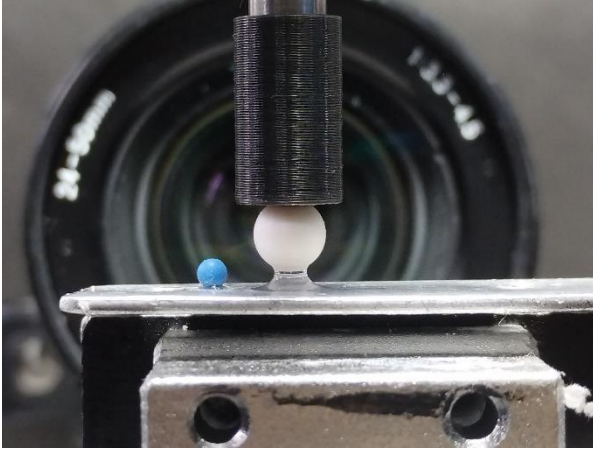


Fig. 1. Photographs of the experimental setup used to vibrate the liquid bridge.

Oscillations are generated by a mechanical oscillator consisting of a motor to which an arm is attached, converting circular motion into horizontal oscillations of the plate. The amplitude, A , is adjusted by varying the position where the arm is fixed, while the frequency, $\frac{\omega}{2\pi}$, is controlled by adjusting the voltage supplied to the motor. Since the particle remains immobile, the lateral deformation of the capillary bridge results from the continuous movement of the base.

Each experiment involves applying a sinusoidal excitation to the aluminum plate at a fixed amplitude and frequency. The continuous motion of the capillary bridge and the base is recorded by a high-speed camera at 500-800 fps. The obtained videos are processed using Matlab©.

Figure 2 shows a typical snapshot at an oscillation frequency of 3.5 Hz and an amplitude of 0.5 mm, corresponding to a low capillary number ($Ca \sim 10^{-5}$). The advancing and receding contact angles (θ_A, θ_R) are determined by analyzing the video frames and using image contrast to define the regions corresponding to the capillary bridge and the particle. Three circles are defined for each image: one for the particle and two for the bridge curvature. The intersection points of these circles are used to calculate the angles by defining tangents to them. Figure 2 indicates the procedure followed by the Matlab© subroutine, which uses the full resolution of the images to measure the angles. Depending on the stage of the movement, either θ_A or θ_R are determined.

3 Results and discussion

Once θ_A and θ_R are determined, they are plotted as a function of the capillary number, defined as:

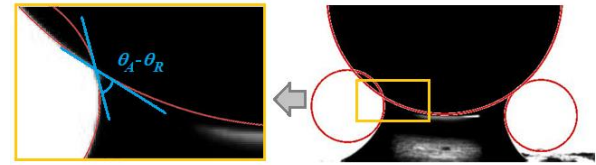


Fig. 2. *Right:* typical snapshot taken as the particle is horizontally vibrated. The circles indicated in red are those determined by the analysis subroutine. *Left:* magnification of the intersecting circles for tangent determination and angles measurements just to illustrate the procedure.

$$Ca = \frac{\mu v}{\sigma} \quad (1)$$

where μ is the liquid viscosity (1.61×10^{-2} P.s for ethylene glycol), v is the velocity of the plate, and σ is the liquid- gas surface tension. Note that the velocity of the plate varies harmonically with time, therefore Ca ranges from 0 to a maximum value equal to $\frac{\mu A \omega}{\sigma}$. In the results presented here, the maximum value attained by the capillary number is 2.3×10^{-3} .

Figure 3 shows the results for the capillary angles as a function of Ca

3.1 Theoretical considerations

As mentioned in the Introduction, previous studies have focused on the capillary torque experienced by a particle rolling on a surface in the presence of a liquid film [9].

In Figure 2, the oscillations of the plane surface cause the liquid bridge between the particle and the plane to deform. If the liquid bridge were not deformed, the advancing and receding angles would be identical and equal to θ_0 .

As soon as the capillary number (Ca) becomes sufficiently small, the theoretical analysis of the behaviour of θ_A and θ_B for a deformed liquid bridge can be accomplished using the Cox-Voinov law [11, 12]. The following equations describe the capillary angles as a function of θ_0 [9]:

$$\theta_A^3 = \theta_0^3 + \alpha Ca \quad (2)$$

$$\theta_R^3 = \theta_0^3 - \alpha Ca \quad (3)$$

where $\alpha = 9 \ln(c \frac{l_k}{l_m})$, with l_k and l_m representing, respectively, characteristic macroscopic and microscopic length scales of the problem. Typically, l_k is related to the capillary length, which for ethylene glycol is of the order of 0.2 cm, while l_m is of the order of the size of a molecule of the liquid involved ($\sim 5 - 6 \times 10^{-8}$ cm for ethylene glycol) [9]. The constant coefficient c is related to geometric characteristics of the system.

At least in the case of constant velocity or acceleration, the above equations can predict the behaviour of the capillary angles as a function of Ca [9, 10, 13]. In the present case, however, the capillary number changes due to the harmonic oscillation of the velocity, and the acceleration of the plate is also varying

harmonically with time. Consequently, we will analyse the validity of this theoretical description in the context of our results in the next subsection.

3.2 Experimental results

Figure 3 presents the results obtained from the analysis of the videos for two complete oscillation cycles, showing the values attained by θ_A and θ_R as a function of time. Note that the “advancing” and “receding” roles of the angles invert with each half-cycle, when the platform reverses its direction of movement.

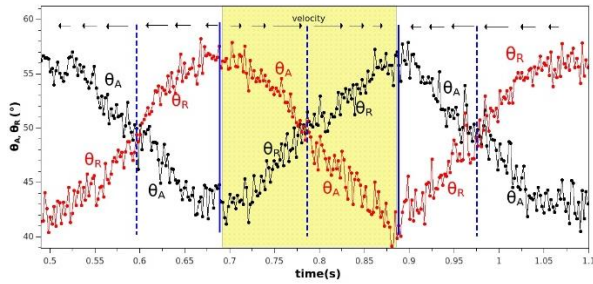


Fig. 3. Values of θ_A and θ_B vs. time. The red curve corresponds to the left side of the bridge, while the black curve represents the right side. The oscillation amplitude is 0.4 mm, and the frequency is 2.65 Hz.

As observed, the oscillatory behaviour of the angles on the left and right sides of the liquid bridge is symmetric when the velocity is reversed. Let us analyse one semi-cycle, such as the one highlighted in Figure 3. To track the different stages of the bridge deformation, we refer to the sketch in Figure 4.

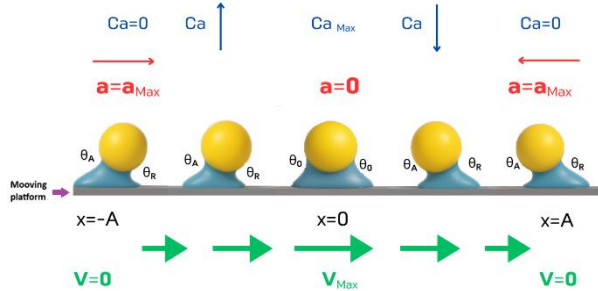


Fig. 4. Schematic representation of successive positions of the liquid bridge and the sphere during the half-cycle highlighted in Figure 3.

During this part of the motion, the particle starts at the leftmost point of the platform trajectory ($x = -A$), with the platform velocity equal to zero and maximum positive acceleration (see Figure 4). As the platform moves in the positive direction, its velocity first increases up to its maximum value, and then decreases to zero again, as indicated in the figure. Considering the relative position of the particle with respect to the platform, the liquid bridge deforms as if the particle were moving to the left relative to a fixed platform. For this reason, the deformation of the bridge is represented by the right-side angle as the receding angle, θ_R , and the left-side angle as the advancing angle, θ_A .

It is important to note that Ca increases as the acceleration is positive, up to $x = 0$. At this position,

both capillary angles reach the static equilibrium value θ_0 , which corresponds, in this system, to an angle of 50° . Therefore, from the leftmost point of the trajectory to its midpoint, θ_A decreases from its maximum value to θ_0 , while θ_R increases from its minimum value to θ_0 .

To relate the deformation of the liquid bridge to the increasing capillary number in this first part of the movement, Figure 5 shows both capillary angles as a function of Ca from $x = -A$ to $x = 0$. Considering Eqs. (2) and (3), we propose a linear fit of the data by plotting θ_R^3 and θ_A^3 as a function of Ca , with fitting parameters θ'_0 and α' . Nevertheless, Eqs. (2) and (3) do not apply directly to this scenario because θ_A decreases with increasing Ca , while θ_R increases with Ca . A change in sign has to be addressed.

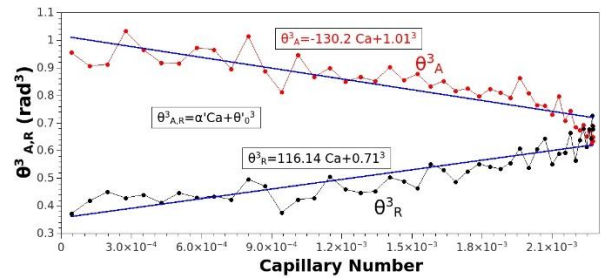


Fig. 5. Behaviour of θ_R^3 and θ_A^3 as a function of Ca during the first part of the half-cycle highlighted in Figure 3. The lines represent the linear fits applied on the experimental data according to Eqs. (2) and (3).

As shown in Figure 5, the experimental data is reasonably well represented by the fitting lines. However, the parameters from the linear regression here differ from those expected in the case of a liquid bridge deformed by a constant velocity motion. For θ_A , the fitting parameter θ'_0 is 57.86° , which corresponds to the maximum value attained by this capillary angle throughout the entire platform trajectory. For θ_R , the fitting parameter θ'_0 is 40.68° , corresponding to the minimum value reached by this angle over the whole trajectory.

Regarding the values for α' , they are $\alpha' = -130$ for θ_A , and $\alpha' = 116$ for θ_R . Considering that $\alpha' = 9 \ln(c \frac{l_k}{l_m})$ and substituting the values of l_k and l_m , it results in c values of 0.56 and 0.12 for θ_A and θ_R , respectively. These values fall within the range expected in the literature [11].

At $x = 0$, Ca starts to decrease as the velocity slows due to the negative acceleration. Nevertheless, the velocity remains positive, and therefore, the angles retain their designations. The behaviour of the capillary angles as a function of Ca in this second part of the analysed region is presented in Figure 6.

Although the behavior of both angles in Figure 6 appears similar to that in Figure 5 and can also be represented with linear fits, we observe different trends: θ_A increases with increasing Ca , while θ_R decreases with Ca . This indicates that Eqs. (2) and (3) directly apply to this scenario. The main difference with the former case is the acceleration, which not only varies but also changes direction at $x = 0$. This implies that the moment exerted by the platform on the capillary bridge

changes sign. Consequently, if the above equations are to be applied in the present problem, the change in sign must be addressed to obtain consistent results.

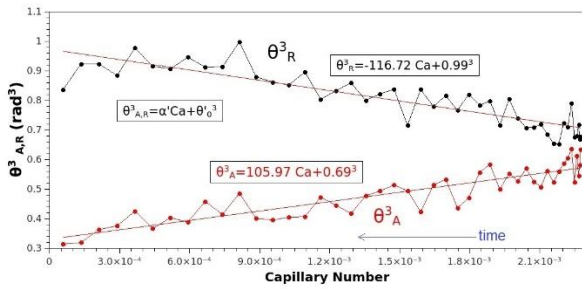


Fig. 6. Behaviour of θ_R^3 and θ_A^3 as a function of Ca during the second part of the half-cycle highlighted in Figure 3. The lines represent the linear fits applied on the experimental data according to Eqs. (2) and (3). Note that the time axis is opposite to the increase of Ca .

It is important to note that in Figure 6, while Ca increases along the horizontal axis, time decreases, as indicated by the arrow. Furthermore, θ_A consistently decreases with time within the analysed region in Figure 3, while θ_R increases with time.

By considering the adequate signs of the respective second terms in Eqs. (2) and (3), we can perform a linear fit of the data in Figure 6. The fitting parameter θ'_0 for θ_A results in 39.53° , corresponding to the minimum value attained by this capillary angle throughout the entire platform trajectory. This is coincident with the minimum value attained by the receding angle at the beginning of the movement. For θ_R , the fitting parameter θ'_0 is 56.72° , corresponding to the maximum value reached by this angle over the whole trajectory, which coincides with the one for θ_A at the initiation of the movement. The values for α' are 106 for θ_A and 117 for θ_R , which, as before, are within the expected range. A similar analysis of the remaining half-cycle yields similar results, confirming the observed behaviour.

4 Conclusion

The deformation of a liquid bridge between a fixed spherical particle and a periodically moving platform was investigated by measuring the advancing and receding capillary angles. The dynamic conditions were maintained at low capillary numbers ($Ca < 10^{-2}$).

The variability in both velocity and acceleration over time distinguishes the present scenario from previously studied cases. As a result, existing equations relating capillary angles and Ca need to be revisited.

We found that the dependence of θ_A and θ_R on Ca changes when the direction of the acceleration reverses. This suggests that the acceleration of the system itself—or equivalently, the rate of change of Ca —is the key factor driving the observed behaviour. Future efforts will focus on developing a new theoretical framework to explain these findings and on exploring the effect on the results when varying the size of the particle and its distance from the surface.

Authors thank Universidad Nacional de San Luis and CONICET for financial support.
 Data is available upon request.
 All authors contributed equally to this

References

1. C.S. O'Hern, Computational Methods, in Handbook of Granular Materials (CRC Press, Taylor & Francis, 2016)
2. J. Duran, Sands, Powders, and Grains: An Introduction to the Physics of Granular Materials (Springer, New York, 2000)
3. S.B. Savage, Disorder, diffusion, and structure formation in granular flows, in Disorder and Granular Media (North Holland, Amsterdam, 1993)
4. S. Herminghaus, Dynamics of wet granular matter. Adv. Phys. **54**, 221–244 (2005)
5. J. Crassous, M. Ciccotti, E. Charlaix, Capillary Force between Wetted Nanometric Contacts and Its Application to Atomic Force Microscopy. Langmuir **27**, 3468–3473 (2011)
6. M. Abdullah, H.D. Rahmayanti, N. Amalia, E. Yuliza, R. Munir, Effective elastic modulus of wet granular materials derived from modified effective medium approximation and proposal of an equation for the friction coefficient between the object and wet granular materials surfaces. Granular Matter **23**, 78 (2021)
7. H. Moharamkhani, R. Sepehrinia, M. Taheri, M. Jalalvand, M. Brinkmann, S. M. Vaez-Allaei, Ordered/disordered monodisperse dense granular flow down an inclined plane: dry versus wet media in the capillary bridge regime. Granular Matter **23**, 62 (2021)
8. J. Chen, J. Shen, J. Guo and G. Wang, Separation efficiency of liquid–solid undergoing vibration based on breakage of liquid bridge. Particuology **61**, 103–110 (2022)
9. J. S. Marshall, Capillary torque on a rolling particle in the presence of a liquid film at small capillary numbers. Chem. Eng. Sci. **108**, 87–93 (2014)
10. P. H. Schade and J. S. Marshall, Capillary effects on a particle rolling on a plane surface in the presence of a thin liquid film. Exp. Fluids **51**, 1645–1655 (2011)
11. O. V. Voinov, Hydrodynamics of wetting. Fluid Dyn. **11**, 714–721 (1976)
12. R. G. Cox, The dynamics of the spreading of liquids on a solid surface. Part I. Viscous flow. J. Fluid Mech. **168**, 169–194 (1986)
13. J. Bico, J. Ashmore-Chakrabarty, G. H. McKinley, H. A. Stone, Rolling stones: The motion of a sphere down an inclined plane coated with a thin liquid film. Phys. Fluids **21**, 082103 (2009)